The NIST Robotic Optical Scatter Instrument (ROSI) and its Application to BRDF Measurements of Diffuse Reflectance Standards for Remote Sensing

Heather J. Patrick,[1,*] Clarence J. Zarobila,[1,2] and Thomas A. Germer[1]
[1]National Institute of Standards and Technology, Gaithersburg MD 20899 USA;
[2]Jung Research and Development Corp., Washington DC 20009 USA

ABSTRACT

We describe the robotic optical scatter instrument (ROSI), a new robotic arm-based goniometer for in-plane and out-of-plane reflectance and bidirectional reflectance distribution function (BRDF) measurements of surfaces. The goniometer enables BRDF measurements to be made at nearly any combination of incident and scattering angles, without obstruction from frames or cradles that occur in traditional goniometers made of nested rotation stages. We present exploratory measurements of in-plane and hemispherically-scanned out-of-plane BRDF on a sintered white polytetrafluoroethylene (PTFE) sample using a supercontinuum fiber laser-based tunable light source operated at a wavelength of 550 nm, in order to demonstrate the capabilities of the system. An initial assessment of uncertainties is presented.

Keywords: BRDF, reflectance, robotics, bidirectional, diffuse, STARR, STARR II, ROSI, supercontinuum

1. INTRODUCTION

The Sensor Science Division of the National Institute of Standards and Technology (NIST) is in the process of expanding its facilities for measuring reflectance and scattering of materials, including measurements of bidirectional reflectance distribution function (BRDF) of diffuse reflectance standards that provide traceability for diffuser plaques used as onboard calibration monitors in remote sensing. The BRDF describes surface reflectance as a function of incident and viewing angles, wavelength, and polarization. For spectrally neutral samples, reflectance and BRDF measurements are currently made using the NIST Spectral Tri-function Automated Reference Reflectometer (STARR).[1] As a calibration service, STARR can measure angle-resolved BRDF for in-plane geometries (where the viewing angle is in the plane formed by the incident angle and the sample normal) from diffuse samples at wavelengths from 250 nm to 1100 nm. While the measurement of angle-resolved BRDF at short-wave infrared (SWIR) wavelengths up to 2500 nm has been demonstrated using STARR, calibrations at wavelengths beyond 1100 nm are presently limited to the normal incidence, 45° viewing (0:45) reflectance geometry.[2,3] In recent years, there has been a growing demand for BRDF measurements at out-of-plane geometries, where the viewing angle is rotated azimuthally from the plane of incidence, at wavelengths from the ultraviolet (UV) to the SWIR. For example, many remote sensing satellites and ground-based remote sensing applications use diffuse reflectors in out-of-plane geometries, and it is highly desirable to calibrate artifacts for these systems in the same geometry as their final use.[4]

Traditionally, at NIST and elsewhere, instruments for measuring in-plane and out-of-plane BRDF at arbitrary incident and viewing angles have used Eulerian cradles or goniometers with nested, orthogonally mounted rotation stages for setting sample orientation, and viewing angles.[5,6] However, in recent years articulated arm robot-based sample positioning systems have been demonstrated.[7,8] Use of a robotic arm allows a clear view of the sample surface out to very high angles, without the obstructing arms or cradles needed to hold orthogonal rotation axes. The robot-based approach also allows direct programming of the sample face orientation using the robot's tool coordinates, and offers high reliability and repeatability.

In this paper, we describe ROSI (the Robotic Optical Scatter Instrument), a new robotic arm-based goniometer for reflectance and BRDF measurements at arbitrary in-plane and out-of-plane viewing geometries. We will give a general description of the instrument, discuss methods for checking alignment and positioning accuracy, and briefly discuss the

* Corresponding author: heather.patrick@nist.gov

Earth Observing Systems XVIII, edited by James J. Butler, Xiaoxiong (Jack) Xiong, Xingfa Gu, Proc. of SPIE
Vol. 8866, 886615 · © 2013 SPIE · CCC code: 0277-786X/13/$18 · doi: 10.1117/12.2023095

optical specifications of the source and receiver being used in the system, which has been described in detail elsewhere.[9,10] Finally, we show the capabilities of the instrument by demonstrating in-plane and hemispherically-scanned BRDF measurements on a sintered PTFE sample. A preliminary assessment of uncertainties for these measurements is also given.

2. SYSTEM DESCRIPTION

2.1 BRDF Measurement Principle

ROSI uses the same BRDF measurement principle that is currently used in STARR. The near-collimated beam from the light source, with incident flux Φ_i, illuminates the sample at a selectable polar angle of incidence, θ_i, and azimuthal angle, ϕ_i, and a receiver collects the scattered flux Φ_r within a solid angle Ω at polar and azimuthal scattering angles θ_r and ϕ_r. Figure 1 shows the coordinate system with the conventions for θ_i, ϕ_i, θ_r and ϕ_r. The BRDF f_r is given by

$$f_r(\theta_i, \phi_i, \theta_r, \phi_r, \lambda, \sigma) = \frac{\Phi_r}{\Phi_i \Omega \cos\theta_r} \quad (1)$$

where the dependence upon wavelength λ and source polarization σ have been shown along with the angular dependence. The units of BRDF are inverse steradian (sr^{-1}). The receiver has a precision aperture of area A, whose center is located a distance D from the center of the illuminated area on the sample. In the limit of small illuminated area and aperture and large distance, the solid angle of collection is given by

$$\Omega = \frac{A}{D^2}. \quad (2)$$

The solid angle in fact varies slightly depending upon illumination and viewing geometry, which is discussed in detail in Ref. 10, and a correction factor is applied when calculating BRDF. Section 5 below will discuss the contribution of illumination area and projected solid angle effects to the uncertainty of our results.

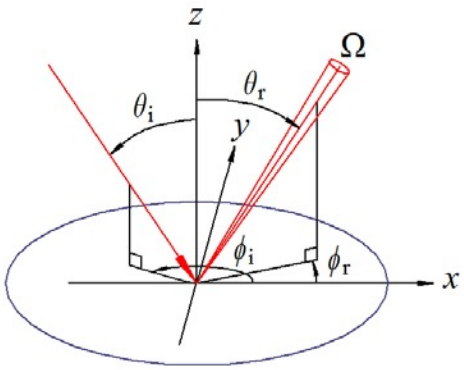

Figure 1: An illustration of the angles used to describe BRDF measurement geometries, where the direction of the beam source and receiver are specified with azimuthal and polar angles in the coordinate frame of the sample surface.

2.2 Goniometer Description

Figure 2 shows a photo of ROSI, and Table 1 summarizes its features. ROSI employs an industrial 6-axis robotic arm (Staubli TX60[†]) for rotation and translation of the sample, and a receiver mounted on an arm connected to a rotation stage that moves the receiver about the central sample position. The robot is programmed such that the area of interest on the sample face is held at the goniometer center, which is defined by the intersection of the incident light beam and

[†] Certain commercial equipment, instruments, software, or materials are identified in this paper to specify the experimental procedure adequately. Such identification is not intended to imply recommendation or endorsement by the National Institute of Standards and Technology, nor is it intended to imply that the materials or equipment identified are necessarily the best available for the purpose.

the robot J1 (waist) rotation axis. The robot and detector arm rotation stage are aligned such that the axis of rotation of the receiver arm is aligned with J1. In this way, a constant distance (*D* in Eq. 1) is maintained between the center of the illuminated area of the sample and the center of the precision aperture of the receiver. The receiver arm is supported by an air bearing that rides on the ground surface of the system table to increase the receiver arm payload and stiffness. For measurements of incident power, the robot moves the sample clear of the incident beam, and the receiver is rotated behind the sample position (to the right in Figure 2). All motion is automated by a LabVIEW program that we are in the process of integrating with our existing LabVIEW controls for the light source and detector electronics.

Figure 2: The Robotic Optical Scatter Instrument (ROSI) positioned for an out-of-plane scattering measurement of a white diffuse sample. Only the robotic arm sample holder and receiver are shown. The light source is on the optical table to the left and is not visible in the photo, although the illuminated area can be seen on the center of the sample.

Samples are held using an integrated vacuum chuck or mechanically attached to the sample holder. This allows most samples to be held by the back face, so that the receiver view of the front of the sample is unobstructed and the sample face does not need to be touched. The thickness of the sample is input to the robot software to bring the sample face to the goniometer center. Wedged samples can also be accommodated in software, provided the direction of the wedge is known. Alternatively, samples which require mounting from the front face can be provided with an adapter that then mounts to the sample holder.

Goniometer Specifications		
Parameter	**Specification**	**Notes**
Robot Type	Articulated Arm	± 0.02 mm positioning repeatability
Number of Axes	6	Enables full hemispherical scanning
Sample size	Up to 12” square	Thickness 0” – 1”, (nominal range, thicker samples considered)
Sample Payload	3.5 kg nominal; 9 kg max	Including sample holder
Sample Attachment	Vacuum chuck or mechanical	Rear or front mount (with adapter)
Sample Translation	± 75 mm from center	Depending upon size
Receiver Arm Rotation	360° about robot	
Receiver Arm Payload	7 kg	
Nominal Receiver Distance	640 mm	
Optical Specifications		
Parameter	**Specification**	**Notes**
Measurement Types	Reflectance, BRDF	In-plane, out-of-plane
Source type	Supercontinuum/monochromator	Other lasers available
Wavelengths	500 nm – 2450 nm tunable	For supercontinuum source, expansion to 250 nm plannned
Wavelength resolution	10 nm	
Incident Beam Diameter	1 cm	Supercontinuum at normal incidence
Polarization	Linear incident	Rotatable
Detector types	Si, Extended InGaAs	Simultaneously operable, located on both the receiver and monitor
Solid Angle of Collection	0.0028 sr	Subtends about 3.8°
Incident angle	θ_i = 0° - 80°, ϕ_i =0° - 360°	Based on 1 cm incident beam
Reflection angle	θ_r= 0° - 90°, ϕ_r =0° - 360°	Full hemispherical scanning, unobstructed view of sample

Table 1: Features of ROSI

2.3 Optical Description

The current light source for ROSI is shown in Figure 3 and has been discussed in detail in Refs. 9 and 10. Its features are also summarized in Table 1. The source consists of a supercontinuum fiber laser with continuous broadband output from below 500 nm to 2450 nm, coupled to a monochromator using an off-axis parabola (OAP) to collimate the fiber output, followed by two translatable lenses L1 and L2, and an order-sorting filter wheel, FW. At the monochromator output, a fused-silica diffuser (DIFF) precedes a round aperture (AP) 500 μm in diameter. The output from the aperture is quasi-monochromatic light of about 10 nm bandwidth that is tunable from 500 nm to 2450 nm.

After the monochromator, a lens (L3) images the aperture to the sample, resulting in a 1-cm diameter circular illumination area at the sample plane when the sample is at normal incidence. Mirrors (M) enable alignment of the source to the goniometer, and automated translation of L3 ensures that the illumination area remains in focus over the broad wavelength range of the source. A chopper (CH) operating at 75 Hz allows lock-in detection of incident and scattered/reflected light during measurements. We control the polarization of the light delivered to the goniometer using a half-wave plate (HWP) and linear polarizer (POL) such that linearly polarized light with a selectable rotation angle is delivered to the sample. The half-wave plate is used primarily for wavelengths between 1800 nm and 2450 nm. While the light from the monochromator is not strongly polarized at wavelengths below 1800 nm, at the longest wavelengths the source is more strongly polarized,[10] and the half-wave plate serves to rotate the plane of polarization to better match that of the linear polarizer angle. Finally a pick-off window (WIN) reflects a small portion of the source output and directs it to a power monitor that consists of a lens, integrating sphere, and silicon and extended InGaAs detectors

attached to the sphere. Use of the monitor allows us to divide out any fluctuations in the source power during measurements.

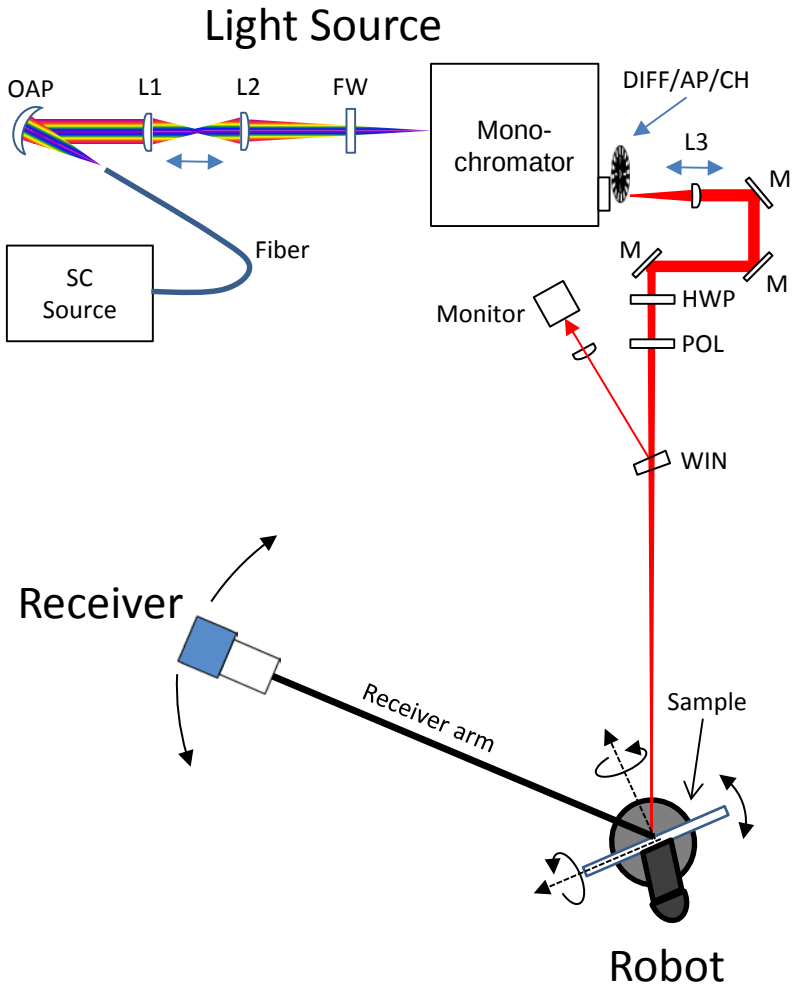

Figure 3: Schematic of the instrument.

The receiver consists of a precision aperture, nominal diameter 38 mm, followed by a CaF_2 lens with appropriate focal length to image a roughly 60 mm diameter field of view at the sample onto the 10 mm entrance port of a small integrating sphere. The 60 mm field of view enables the entire illuminated area on the sample, which spreads to an ellipse for non-zero θ_i, to under fill the receiver field stop for θ_i up to 80°. Two photodiodes, a silicon photodiode with response from 190 nm to 1100 nm and an extended-InGaAs with response from 500 nm to roughly 2500 nm, are mounted on the sphere. ROSI performs absolute measurements of BRDF and reflectance, meaning that the receiver must be able to measure both the incident power and the scattered power. During the incident power measurement, the robot moves the sample clear of the incident beam, the receiver faces the incident beam, and the spot size of the incident beam underfills the precision aperture. In this case, the lens focuses the incident beam into the sphere.

For future measurements, including those below 500 nm and into the UV range of the spectrum, we also have tunable lasers that can be coupled to the goniometer and viewed by the receiver. One promising source is a frequency-doubled and -tripled tunable Ti:Sapphire laser. The use of this source will allow us to access additional wavelengths from 230 nm to 500 nm.

3. ROBOT MOTION AND ALIGNMENT

In this section, we briefly describe how sample motions are input to the robot, and discuss alignment tools for verifying these motions.

3.1 Robot reference frames

Figure 4 shows the location of the robot J1 and the receiver arm D1 motions. At installation, the rotation axes of J1 and D1 were set to be coincident by mechanical alignment of the robot base and receiver arm rotation stages. The robot software accepts the definitions of multiple coordinate systems, built upon one another. We define a home reference frame with its origin at a point along the J1 axis at the height of the incident beam as shown in the figure. The home reference frame z axis points back along the incident beam, its x axis is along the J1 rotation axis, and the y axis is perpendicular to x and z such that the axes form a right-handed coordinate system. Sample rotations are input with respect to this home orientation, first applying the yaw angle about x, then pitch about the (now rotated in yaw) y axis, and finally roll about the yawed and pitched z axis. Following Ref. 10, this combination of pitch, yaw, and roll, along with the receiver rotation D1, allow the goniometer to bring a sample to any combination of sample-centered incident and view angles θ_i, ϕ_i, θ_r and ϕ_r.

Once the goniometer home frame is defined, the second step is to define the sample face location and orientation with respect to the hand flange of the robot. The sample is considered a "tool" attached to the hand flange. The offset and orientation of the sample face relative to the hand flange are determined and input to the robot's control software. Once the sample offset and orientation are stored in the robot, they become a new sample face frame of reference. The origin and axes of the sample frame can be brought to be coincident with the home frame, or rotated with respect to the home frame to achieve desired incident and view angles on the sample. Samples of different thicknesses are accommodated by changing the sample frame offset in software. Wedge can also be accommodated by changing the angle of the sample frame relative to the hand flange frame.

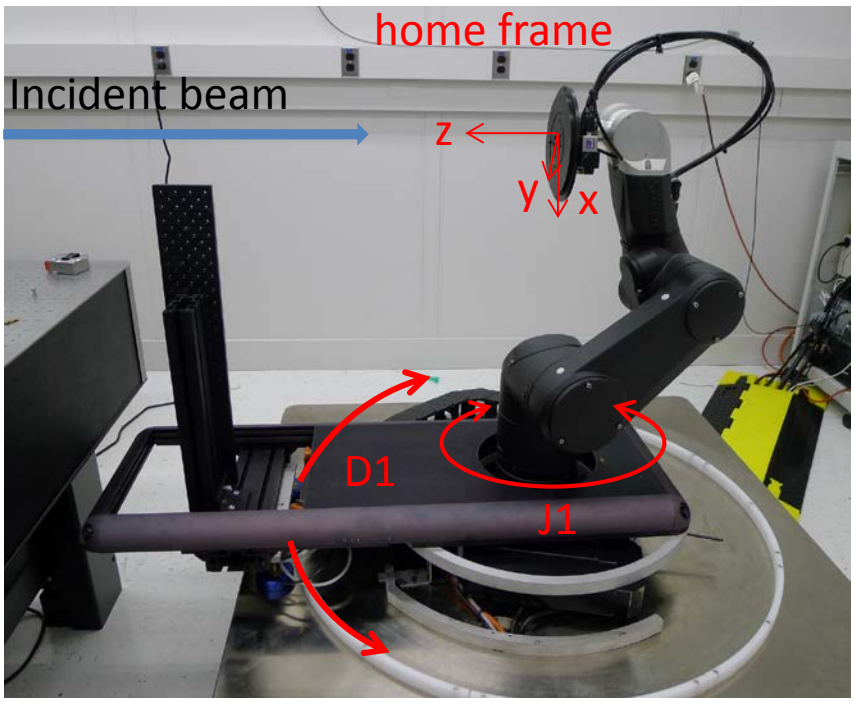

Figure 4**:** Robot with sample holder in the home position, showing the orientation of the home reference frame axes. The rotations of the J1 (robot waist) and D1 (receiver arm rotation stage) are also shown.

3.2 Defining the home and sample frames

Aligning the system consists of correctly defining the home frame to match the incident beam height and direction, and determining the offsets of the sample face from the robot hand flange. It is also important to be able to verify the concentricity and angle agreement of the J1 and D1 axes.

To aid in and check alignment of the robot goniometer at the micrometer level, we used a non-contact eddy current probe (Micro-Epsilon NCDT3010). The sensor produces a near-linear output of voltage versus displacement between the sensor and a metallic target, over a maximum operating range of 1 mm and 0 V to 10 V. We estimate the working accuracy of the eddy sensor for displacement to be 11.0 V/mm ± 0.6 V/mm as long as the central 0.5 mm (voltage outputs from 2 V to 8 V) are used.

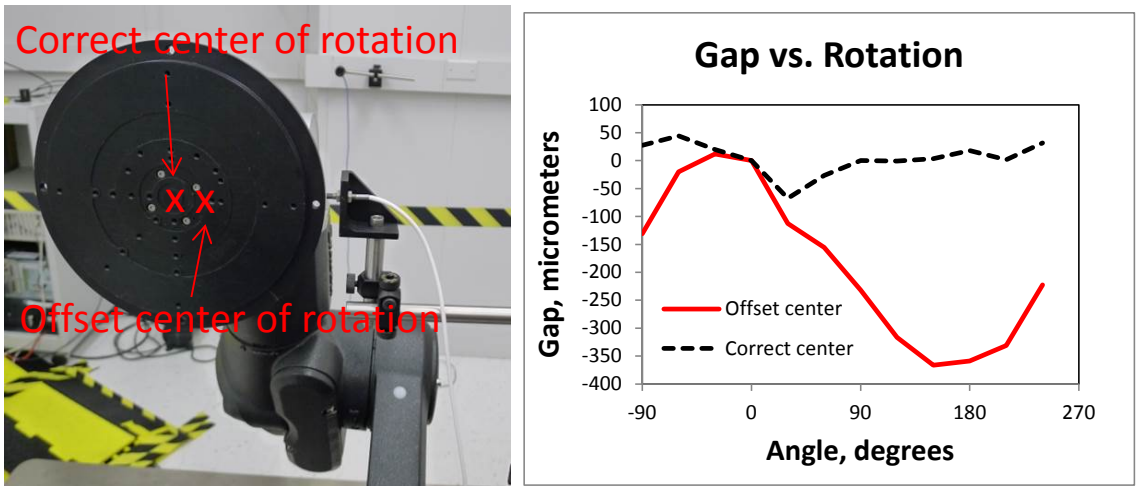

Figure 5: Eddy sensor gap versus sample roll when the sample center of rotation is at the center of the sample holder (black dashed line) and when the center of rotation is offset horizontally from the sample holder center (red solid line).

Figure 5 shows an example alignment performed using the eddy sensor. As part of the determination of the correct offset of the sample center with respect to the hand flange, we positioned the eddy sensor along the edge of the sample holder and input a roll rotation of the sample with respect to the home frame. If the sample offset is incorrect, the sample holder will be rolled about a point offset from its center, which will appear as runout on the eddy sensor. Figure 5 shows the measured runout (gap) for the correct centering (dashed line) and for a case where the sample center was offset in the horizontal direction from the actual sample center. Use of the eddy sensor allows the correct center point to be determined.

We also use the eddy sensor to verify the centering of the robot J1 (waist axis) and receiver arm D1 rotation axis. In this case, we faced the sample holder directly towards the receiver arm, extended a beam from the sample holder face such that the eddy sensor was within 1 mm of a surface on the receiver arm, and then simultaneously rotated J1 and D1 through 360° and recorded the change in the eddy sensor gap. The measured runout was ± 35 μm peak-to-peak, which gives a small (but not negligible) contribution to the distance uncertainty. We present this as an example of the use of the eddy sensor for alignment checks, not as an exhaustive survey of the goniometer alignment. We are continuing to evaluate the goniometer alignment using the eddy sensor and other methods.

4. MEASUREMENTS

4.1 In-plane BRDF of sintered PTFE

As an initial demonstration of the use of the instrument for BRDF, we performed in-plane BRDF measurements on a sample of sintered white PTFE. The results are shown in Fig. 6. For these measurements, the light source was set at a wavelength of 550 nm, and incident with $\phi_i = 180°$. Points with negative θ_r correspond to scattering angles on the incident side of the sample normal ($\phi_r = 180°$), while those with positive θ_r have $\phi_r = 0°$. The missing data points indicate angles where the receiver blocked the incident beam. The BRDF at each incident angle was measured for two polarizations, horizontal and vertical, and the results averaged to give the effective unpolarized BRDF shown in the plot.

These measurements should be considered preliminary and have not been compared with other NIST instruments. For 0:45 BRDF, they are in general agreement with previously published values.[11] The BRDF values for $\theta_i = 0°$, where one would expect a symmetric BRDF if there were no anisotropy in the scattering from the sample, are slightly higher overall on the positive θ_r side of the sample. Initial investigation (rolling the sample, in other words, changing ϕ_r while keeping θ_r fixed) indicates there is anisotropy in the sample itself, and this will be explored further in future measurements when the system is more completely automated. The apparent anisotropy points to the need to have a fiducial mark on the sample specifying its mounting orientation with respect to the sample holder/sample coordinates. The increasing BRDF with high view angles on the specular side of the sample seen for $\theta_i = 60°$ and $\theta_i = 45°$ is characteristic of PTFE at high incident angles.

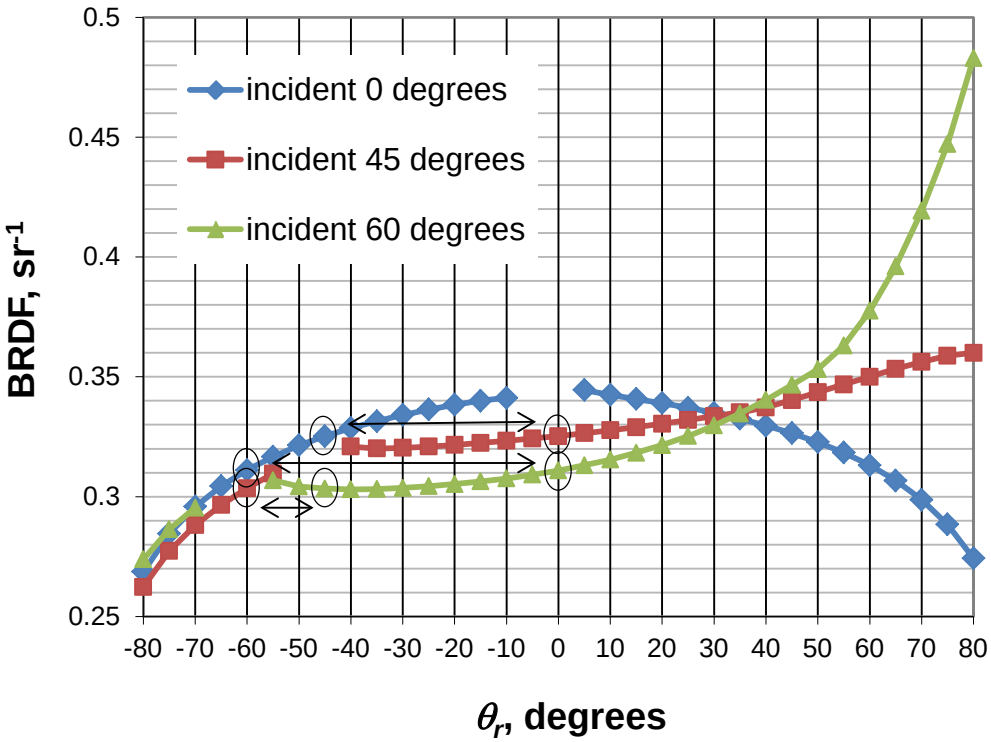

Figure 6**:** In-plane BRDF of a sintered PTFE sample for unpolarized light at 550 nm, taken every 5°. The circled points with connecting arrows indicate angles that are expected to have the same BRDF due to reciprocity.

We are encouraged by the good reciprocity shown in the data; that is, the BRDF is the same when scattering and incident angles are interchanged. The circled points connected by arrows in Fig. 6 represent points where incident and viewing angles are directly interchanged: $\theta_i = 45°$, $\theta_r = 0°$ with $\theta_i = 0°$, $\theta_r = -45°$, $\theta_i = 60°$, $\theta_r = 0°$ with $\theta_i = 0°$, $\theta_r = -60°$, and $\theta_i = 45°$, $\theta_r = -60°$ with $\theta_i = 60°$, $\theta_r = -45°$. As seen in the figure, agreement between these points was very good. In the worst case, the BRDF disagreed by 0.0002 sr^{-1}.

4.2 Hemispherically-scanned BRDF

For this measurement, we used the out-of-plane scanning capability of ROSI to measure the BRDF as a function of polar and azimuthal scattering angles, θ_r and ϕ_r, at a fixed incident angle of θ_i = 60° and ϕ_i = 180°. We used the transformations of Ref. 10 to convert the desired sample frame angles θ_i, ϕ_s, θ_r and ϕ_r to the appropriate sample orientation and receiver rotation. At each viewing position, the BRDF was obtained. As in the in-plane measurements, two polarizations, horizontal and vertical, were used, and the results averaged to obtain the BRDF shown on the plot. We chose a grid of θ_r and ϕ_r that gave a spacing of 0.2 in direction cosine space, which is defined by

$$x = \sin\theta_r \cos\phi_r \quad (4)$$

$$y = \sin\theta_r \sin\phi_r \quad (5)$$

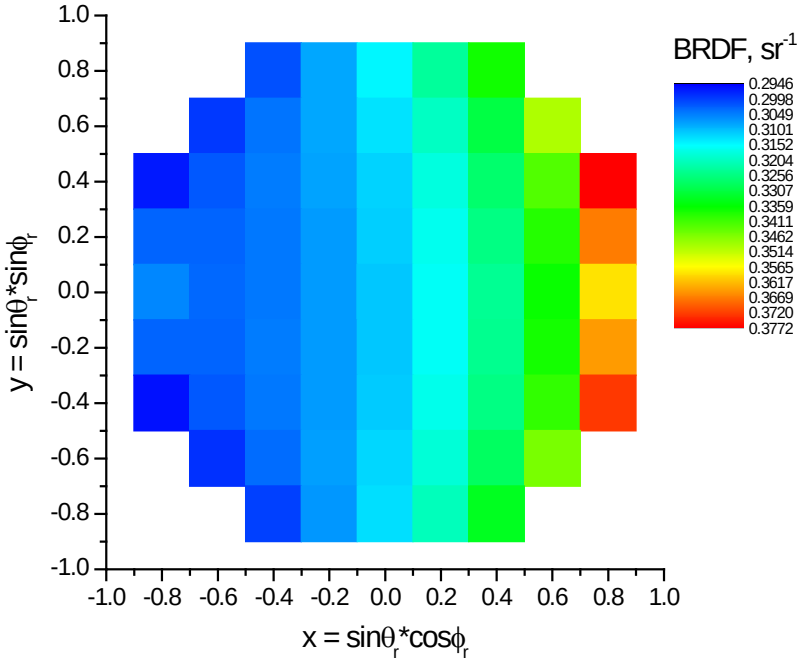

Figure 7**:** Hemispherically scanned BRDF of a sintered PTFE sample for unpolarized light at 550 nm incident from the θ_i = 60° and ϕ_i = 180° direction, plotted in direction cosine space.

Direction cosine space provides a 2-dimensional view of the hemispherical scattering as if one were looking down on the scattering pattern from above. The radial position corresponds to the polar angle θ_r, while the azimuthal angle is zero along the +x axis and increases with counter-clockwise rotation. Thus in-plane measurements are along the x-axis. In future measurements, using even spacing in direction cosine space will simplify the integration of hemispherically scanned BRDF to total hemispherical BRDF.[12]

From the graph, the in-plane BRDF (along the x-axis with y=0) is in very good agreement with the in-plane measurement of Figure 6. The in-plane angles in Fig. 7 range from θ_r = -53.5° to θ_r = 53.5° and over that range, the in-plane BRDF of Fig. 7 and Fig. 6 agreed to better than 0.2% at all points. This indicates that the day to day reproducibility of the robot goniometer is very good. Out-of-plane, the data demonstrate the clear non-lambertian behavior of sintered PTFE and the need to provide customers with calibrations at out-of-plane geometries. For example, the BRDF at x = 0.6, y = 0, corresponding to the angles θ_r = 36.9° ϕ_r = 0°, is 0.3367 sr^{-1} while that at the same polar angle but -90° view (x = 0, y = -0.6, or θ_r = 36.9° ϕ_r = -90°) is 0.3122 sr^{-1}. As already noted, a fiducial mark should be given such that the sample is measured with the same orientation with respect to the incident beam that will be used by

the customer. Uncertainty analysis and validation for out-of-plane measurements are ongoing. The non-lambertian behavior observed here is in qualitative agreement with other results.[5]

5. UNCERTAINTY CONSIDERATIONS

The measurement equation for BRDF given in Eq. (1) provides a good starting point for evaluation of the uncertainties in a BRDF measurement. A more exhaustive study of the uncertainties in ROSI is planned when automation of the system is complete. We first modify Eq. (1) to include the correction for incident beam profile, finite illumination and aperture effects[10] as

$$f_{\mathrm{r}}(\theta_{\mathrm{i}}, \phi_{\mathrm{i}}, \theta_r, \phi_r, \lambda, \sigma) = \frac{1}{C} \cdot \frac{\rho D^2}{A \cos \theta_{\mathrm{r}}} \tag{6}$$

where we define the ratio of scattered optical power to incident optical power as

$$\rho = \frac{\Phi_r}{\Phi_i} \tag{7}$$

and where C is the illumination and aperture correction. The optical powers Φ_r and Φ_i at the goniometer receiver are measured using a solid state detector (only the Si detector was used for this work), pre-amp, and lock-in amplifier. In addition a monitor channel, with its own detector, pre-amp, and lock-in amplifier, is used to divide out any drift in the light source power. Therefore in practice we measure ρ as

$$\rho = \frac{\mathrm{V}_{scat,r}}{\mathrm{V}_{scat,m}} * \frac{\mathrm{V}_{inc,m}}{\mathrm{V}_{inc,r}} * GR * SL \tag{8}$$

Here $V_{scat,r}$ and $V_{scat,m}$ are the voltages read by the receiver and monitor lock-ins during the scattered power measurement and $V_{inc,r}$ and $V_{inc,m}$ are the voltages read by the receiver and monitor lock-ins during the incident power measurement. Because we change the gain of the receiver pre-amp and the sensitivity of the receiver lock-in between measurements of incident power and scattered power, we also include *GR*, the ratio of the receiver pre-amp gain (read in volts/amp) during the incident power measurement to the receiver pre-amp gain during the scattered power measurement, and *SL*, which accounts for any difference in the voltage response of the lock-in at the sensitivity settings used during the scattered and incident power measurements. Assuming for the moment that all components of the measurement equation are uncorrelated, we then have the uncertainty in f_r, $u(f_r)$, given by[13]

$$\frac{u^2(f_r)}{f_r^2} = \frac{u^2(V_{scat,r})}{V_{scat,r}^2} + \frac{u^2(V_{scat,m})}{V_{scat,m}^2} + \frac{u^2(V_{inc,m})}{V_{inc,m}^2} + \frac{u^2(V_{inc,r})}{V_{inc,r}^2} + \frac{u^2(GR)}{GR^2} + \frac{u^2(SL)}{SL^2} + \frac{u^2(C)}{C^2} + \frac{4u^2(D)}{D^2} + \frac{u^2(A)}{A^2} + (\tan\theta_r)^2\, u^2(\theta_r) \tag{9}$$

In Table 2, we give estimate the relative standard uncertainty of each of the components, for one polarization of the in-plane, angle of $\theta_i = 0°$ and $\theta_r = 45°$ measurement shown in Fig. 6, and the corresponding relative expanded uncertainty in f_r using Eq. 9, which is currently dominated by geometric and alignment effects. We expect that, as we continue to improve our knowledge of the instrument's capabilities and explore sources of systematic error, these values will change. In general some, if not most, sources of uncertainty will depend on the sample and measurement requested. For example, the explicit scaling of the scattering angle component with $\tan(\theta_r)$ means that measurements at higher viewing angles will have larger uncertainty. In other cases, measurements at wavelengths where the source power is greater may have smaller uncertainty in scattered power measurement due to better signal to noise on the detector. We also have to consider sample effects. Fig. 6 suggests that the sample we measured has a BRDF at $\theta_i = 0°$ that varies with ϕ_r. It is also very difficult to determine if there is any wedge to a diffuse sample, or its flatness. For sample distance, we considered u(D) to be a fairly conservative ± 0.2 mm. While the goniometer alignment discussed in Section 3 suggests that the robot to receiver distance remains constant to much better than this, we increased the distance uncertainty because of the difficulty in determining the diffuse sample thickness to better than 0.1 mm, uncertainty in determining the location of the precision aperture edge relative to the flat measuring surface available on the face of the receiver, and so on. We estimated the angle uncertainty, u(θ_r), at a nominal ± 0.02° but this assessment is also ongoing. The uncertainty in correction to measured BRDF based upon illumination and aperture effects $u(C)$ is dominated by our ability to align the incident beam through the center of the goniometer, with even slight misalignment able to shift the beam off center by

tenths of millimeters. We estimate the beam was centered to within ± 0.2 mm which gives $u(C)/C$ of 0.05% for the 0:45 geometry.[10] Finally, we have not yet included effects that do not appear directly in the measurement equation, but depending on the BRDF characteristics of the sample, may be significant. These include stray light, wavelength uncertainty (for samples with wavelength dependent BRDF), uncertainty in incident angle, polarization dependence in the receiver, and others.

Parameter	**Component**	**Value**
Receiver voltage, scattered power measurement	$u(V_{scat,r})/V_{scat,r}$	0.021 %
Monitor voltage, scattered power measurement	$u(V_{scat,m})/V_{scat,m}$	0.013 %
Receiver voltage, incident power measurement	$u(V_{inc,r})/V_{inc,r}$	0.011%
Monitor voltage, incident power measurement	$u(V_{inc,m})/V_{inc,m}$	0.010%
Receiver Pre-amp gain ratio	$u(GR)/GR$	0.005%
Lock-in response	$u(SL)/SL$	0.024%
Finite Illumination/Aperture Correction	$u(C)/C$	0.050%
Sample distance	$2*u(D)/D$	0.063 %
Aperture area	$u(A)/A$	0.0008 %
Scattering angle	$u(\theta_r)tan(\theta_r)$	0.035%
Total Relative Expanded Uncertainty (k=2)	$2*u(f_r)/f_r$	0.19%

Table 2: Summary of currently identified uncertainty components for a BRDF measurement at θ_i = 0° and θ_r = 45° in-plane on a white sintered PTFE sample at 550 nm.

6. SUMMARY AND FUTURE WORK

We have reported on the status of ROSI, a new robotic-arm based goniometer for reflectance and BRDF measurements. The instrument has been shown to be capable of in-plane and out-of-plane BRDF measurements, and details of the robot motion control, assessment of alignment, and operation with a supercontinuum-based, tunable light source have been discussed. Considerations for the accurate measurement of BRDF with this source and a robotic arm-based goniometer have been presented, and preliminary uncertainty estimates discussed. Future work is expected to include completion of the LabVIEW automation integrating source and goniometer control, installation of the extended InGaAs detectors that enable SWIR measurements, extension to UV wavelengths, and detailed characterization of systematic and random sources of error. Comparisons with STARR are also planned.

7. REFERENCES

1. Proctor, J.E. and Barnes, P.Y., "NIST high accuracy reference reflectometer-spectrophotometer," J. Res. Natl. Inst. Stand. Technol. 101, 619-627 (1996). See also http://www.nist.gov/pml/div685/grp03/spectrophotometry_starr.cfm.
2. Yoon, H.W., Allen, D.W., Eppeldauer, G.P., and Tsai, B.K., "The extension of the NIST BRDF scale from 1100 nm to 2500 nm," Proc. SPIE 7452, 745204 (2009).
3. Tsai, B.K, Allen, D.W., Cooksey, C., Yoon, H.W., Fulton, L., Biggar, S., and Markham, B., "Calibration of LANDSAT/OLI Panels Using the NIST BRDF Scale from 1100 nm to 2400 nm," CALCON Technical Conference, Logan, Utah, 2010.
4. A survey of remote sensing satellites can be found at http://www.crisp.nus.edu.sg/~research/tutorial/optical.htm
5. Obein, G., Bousquet, R., and Nadal, M.E., "New NIST Reference Goniospectrometer," Proc. SPIE 5880, 58800T1-10 (2005).
6. http://www.nist.gov/pml/div685/grp06/scattering_bidirectional.cfm
7. Huenerhoff, D., Grusemann, U., and Hoepe, A., "New robot-based gonioreflectometer for measuring spectral diffuse reflection," Metrologia **43**, S11-S16 (2006).
8. Baribeau, R., Neil, W.S., and Côté, E., "Development of a robot-based gonioreflectometer for spectral BRDF measurement," Journal of Modern Optics, 56: 13, 1497-1503 (2009).

9. Zarobila, C.J., and Patrick, H.J., “Supercontinuum fiber laser source for reflectance calibrations in remote sensing,” Proc. SPIE 7807, 78070B-1-17 (2010).
10. Patrick, H.J., Zarobila, C.J., Germer, T.A., Ying, V.A., Cooksey, C.A., and Tsai B.K., “Tunable Supercontinuum Fiber Laser Source for BRDF Measurements in the STARR II Gonioreflectometer,” Proc. SPIE 8495, 84950K-1 (2012).
11. Barnes, P.Y., and Early, E.A., “Diffuse reflectance of sintered and pressed polytetrafluoroethylene (PTFE),” Proc. SPIE 3426, 190 (1998).
12. Patrick, H.J., Hanssen, L.M., Zeng, J., and Germer, T.A., “BRDF measurements of graphite used in high-temperature fixed point blackbody radiators: a multi-angle study at 405 nm and 658 nm,” Metrologia 49, S81-92 (2012).
13. Taylor, B.N. and Kuyatt, C.E., “Guidelines for Evaluating and Expressing the Uncertainty of NIST Measurement Results,” NIST Technical Note 1297 (1994).